Hyperkeratinization and Proinflammatory Cytokine Expression in Meibomian Glands Induced by *Staphylococcus aureus*

Hua Chen, Hui Gao, Hua-Tao Xie, Shu-Ting Liu, Yu-Kan Huang, and Ming-Chang Zhang

Department of Ophthalmology, Union Hospital, Tongji Medical College, Huazhong University of Science and Technology, Wuhan, China

Correspondence: Yu-Kan Huang, Department of Ophthalmology, Union Hospital, Tongji Medical College, Huazhong University of Science and Technology, No. 1277 Jiefang Avenue, Wuhan 430022, Hubei Province, China; whuh_huangyk@163.com.
Ming-Chang Zhang, Department of Ophthalmology, Union Hospital, Tongji Medical College, Huazhong University of Science and Technology, No. 1277 Jiefang Avenue, Wuhan 430022, Hubei Province, China; mingchangzhang@hotmail.com.

Received: February 23, 2021
Accepted: September 15, 2021
Published: October 13, 2021

Citation: Chen H, Gao H, Xie HT, Liu ST, Huang YK, Zhang MC. Hyperkeratinization and proinflammatory cytokine expression in meibomian glands induced by *Staphylococcus aureus*. *Invest Ophthalmol Vis Sci.* 2021;62(13):11. https://doi.org/10.1167/iovs.62.13.11

Purpose. This exploratory study aimed to investigate the morphological and pathological alterations of the meibomian gland (MG) with the *Staphylococcus aureus* crude extracts (SACEs) treatment.

Methods. Mouse MG explants were cultured and differentiated with or without SACEs for 48 hours. Explant's viability and cell death were determined by thiazolyl blue tetrazolium bromide (MTT) assay and TUNEL assay. MG morphology was observed by Hematoxylin and Eosin staining. Lipid droplet production was detected by Nile Red staining and LipidTox immunostaining. The pro-inflammatory cytokines were detected by ELISA. The relative gene and protein expression in MG explants was determined via quantitative RT-PCR, immunostaining, and immunoblotting. The components of the SACEs were analyzed by immunoblotting and silver staining.

Results. Our findings demonstrated that the SACEs treatment induced overexpression of keratin 1 (Krt1) in the ducts and acini of MG explants, accompanied by a decrease in viability and an increase in cell death in explants. Furthermore, the SACEs treatment dose-dependently increased the levels of TNF-α, IL-1β, and IL-6 in MG explants. The SACEs treatment induced activation of the nuclear factor kappa B (NF-κB) and AIM2 (absent in melanoma 2)/ASC (apoptosis-associated speck-like protein containing a caspase recruitment domain) inflammasome signaling pathway in explants. Further investigation showed expression of the key adipogenesis-related molecule peroxisome proliferator-activated receptor γ was decreased after SACEs treatment. However, no change was found in the lipid synthesis of MG explants after treatment with the SACEs. Staphylococcal enterotoxins B (SEB) was detected in the SACEs. SEB induced the overexpression of Krt1 and IL-1β in ducts and acini of MG explants.

Conclusions. Our findings confirm that *Staphylococcus aureus* induced hyperkeratinization and pro-inflammatory cytokines expression in MG explants ducts and acini. These effects might be mediated by SEB. Activation of the NF-κB and AIM2/ASC signaling pathway is involved in this process.

Keywords: mouse meibomian gland explants, *Staphylococcus aureus*, meibomian gland dysfunction

As a particular holocrine sebaceous gland unit of the human body, meibomian gland (MG) are embedded in the tarsal plates of both upper and lower eyelids.[1] MG secretes lipids to the tear film, preventing tear evaporation and forming an optically smooth ocular surface, thus maintaining excellent visual acuity.[2] Meibomian gland dysfunction (MGD), a causative factor in evaporative dry eye disease, results in lacrimal film destabilization and increases tear film evaporation and osmolarity.[3–5]

MGD also promotes bacterial growth on the eyelid margin and inflammation of the conjunctiva (e.g., blepharokeratoconjunctivitis, anterior blepharitis, keratitis, posterior blepharitis).[3] Compared with normal subjects, patients with MGD had a higher bacteria culture-positive rate.[6] The abundance of aerobes and anaerobes from both conjunctiva cul-de-sac and lid margin in MGD patients were both higher than in normal individuals.[6–9] It is particularly noteworthy that under 16S rDNA gene sequencing, the positive rate of *Staphylococcus aureus* isolated from the conjunctival sac and MG was significantly higher in MGD patients than in healthy people.[10] Furthermore, *S. aureus* was found to be the major microbiome in patients with MGD.[10]

S. aureus secretes many exotoxins and enzymes or forms biofilms that cause skin and tissue infections.[11] Some previous studies showed that the degree of MG loss in these severe MGD patients was positively correlated with the abundance of *S. aureus*.[12] Several clinical studies have also reported that bacterial lipase and toxin could lead to changes in meibum composition.[13,14] However, there are only a few studies evaluating the effect of *S. aureus* on the MGs. We

hypothesize that *S. aureus* could directly affect MG morphology and physiology. The main goal of this study was to test that hypothesis.

Materials and Methods

Materials

Ki67 (ab16667); keratin 1 (Krt1; ab185628); Alexa Fluor 594, Donkey Anti-Rabbit IgG H&L (ab150076); Alexa Fluor 488, Donkey Anti-Rabbit IgG H&L (ab150105); and lysosomal-associated membrane protein 1 (LAMP-1; ab24170) antibodies were obtained from Abcam (Cambridge, UK). Peroxisome proliferator-activated receptor γ (PPAR-γ) antibody (ARG55241) was obtained from Arigo (Hamburg, Germany). IL-1β antibody (A1112) was obtained from ABclonal (Wuhan, China). Apoptosis-associated speck-like protein containing a caspase recruitment domain (ASC, 67824), phosphorylated nuclear factor kappa B (phospho-NF-κB) p65 (3033), β-actin (4970S), glyceraldehyde-3-phosphate dehydrogenase (GAPDH) (8884), IL-1β (31202S), pro-IL-1β (63124S), caspase-1 (24232), pro-caspase-1 (24232), absent in melanoma 2 (AIM2; 63660), anti-mouse IgG, horseradish peroxidase (HRP)-linked antibody (7076), and anti-rabbit IgG, HRP-linked antibody (7074) were obtained from Cell Signaling Technology (Danvers, MA, USA). Anti-SEB antibody (ITI026624) was obtained from ITI BioChem (Ashland VA, USA), and 4′,6-diamidino-2-phenylindole (DAPI) (28718-90-3) was obtained from Roche Diagnostics (Basel, Switzerland).

Animals

C57BL/6 male mice (4-6 weeks old) were purchased from the Laboratory Animal Center of Tongji Medical College of Huazhong University of Science and Technology (Wuhan, China). All animal procedures were in accordance with the ARVO's Statement for the Use of Animals in Ophthalmic and Vision Research.

Staphylococcal Crude Extract Preparation

S. aureus ATCC29213 was obtained from BeNa Culture Collection (Beijing, China). The *S. aureus* was inoculated in tryptic soy broth (BeNa Culture Collection) and vigorously shaken at 37°C overnight (12–18 hours). For growth curves, pre-warmed tryptic soy broth was inoculated with an overnight culture at an initial optical density of 0.05 or 0.1 at an optical density (OD) of 578 nm (BioTech Instruments, Winooski, VT, USA) and then grown at 37°C with shaking. Bacterium suspensions were taken at regular intervals to detect their OD of 578 nm at 0, 3, 5, 7, and 24 hours. Preparation of the *Staphylococcus aureus* crude extracts (SACEs) method was based on a previous protocol[15] with some minor changes. Briefly, bacteria were collected by centrifugation and rinsed in ice-cold 20-mM Tris-HCl and 100-mM NaCl (pH 8.0) and resuspended in 2 mL of PBS buffer with 1 $\times$ 10^5 U lysozyme (ST206; Beyotime Biotechnology, Shanghai, China) and 1-mm grinding beads (G0101-200G; Servicebio, Wuhan, China). After vortexing and ultrasonic crushing, SACEs were obtained by centrifugation at 10,000 revolutions per minute for 10 minutes at 4°C followed by filtration with a 0.22 µm filtration membrane (723-2520; Thermo Fisher Scientific, Waltham, MA, USA). Protein concentration was measured using a bicinchoninic acid (BCA) assay kit (23225; Thermo Fisher Scientific). Freshly prepared SACEs were kept at –80°C.

Mouse Meibomian Gland Explants Culture

The culture of MG explants was based on a previous protocol[16] with some minor changes. Briefly, MG explants were placed on 24-well plates with the conjunctival side up and cultured in Defined keratinocyte serum-free medium (DKSFM; 10744019; Thermo Fisher Scientific) without using any antibiotics. For western blotting analysis, hair follicles of MG explants were removed by insulin needles. The MG explants were treated with SACEs (0.5, 1, or 2 µg/mL), staphylococcal enterotoxins B (SEB; BT202, 0.5 µg/mL, according to a study on skin explants[17]; Toxin Technology, Sarasota, FL, USA), or PBS (as vehicle control) for 48 hours. All explants were cultured in a water-saturated atmosphere of 5% CO_2 at 37°C.

Thiazolyl Blue Tetrazolium Bromide Assay

Thiazolyl blue tetrazolium bromide (MTT) assays evaluated the viability of the explants as previously described.[16] Briefly, MTT solution was prepared by dissolving 3-(4,5-dimethylthiazol-2-yl)-2,5-diphenyltetrazolium bromide (88417; Sigma-Aldrich, St. Louis, MO, USA) in fresh DKSFM medium at 1 mg/mL. Following various concentrations of treatment, the explants were incubated in 500 µL MTT solution for 4 hours. The MTT solution was then removed, and MTT formazan was dissolved in 500 µL dimethyl sulfoxide (D2650; Sigma-Aldrich) for 10 minutes. Eluate of each sample (100 µL) was transferred to 96-well plates (n = 3 replicates), and OD readings were taken at 490 nm (BioTech Instruments).

Histology

The MG explants were fixed with 4% paraformaldehyde (P0099; Beyotime Biotechnology) for 1 hour at 37°C. For paraffin sections, explants were dehydrated through graded alcohols and embedded in paraffin wax until sectioning (8 µm). Hematoxylin and eosin (H&E) staining was performed on the paraffin sections for morphological observation on a DFC550 microscope (Leica Microsystems, Wetzlar, Germany). For frozen sections, explants were embedded in optimal cutting temperature compound, cut into sections (10 µm), and then stored at –80°C. TUNEL assays, immunofluorescence staining, Nile Red (19123; Sigma-Aldrich) staining, and LipidTOX (H34475; Thermo Fisher Scientific) staining were performed on the frozen sections.

Nile Red Staining and LipidTOX Staining

Frozen microtomes were stained with freshly prepared Nile Red or LipidTOX solution for 30 minutes at room temperature. After washing with PBS for 15 minutes, the sections were counterstained with DAPI for 15 minutes, followed by washing with PBS for 15 minutes. Images were then acquired with a laser scanning confocal microscope (A1 HD25/A1R HD25; Nikon, Tokyo, Japan). The mean intensity of staining in sections was measured by image analysis software (NIS-Elements Viewer 4.50; Nikon).

Investigative Ophthalmology & Visual Science

TUNEL Assay

TUNEL staining was performed on 10-µm cryosections and detected using the *In Situ* Cell Death Detection Kit, Fluorescein (11684795910; Roche Diagnostics). Briefly, the explant sections were stained in 50 µL of TUNEL reaction mixture for 1 hour at 37°C in the dark. The specimens were washed three times with PBS for 5 minutes, and nuclei were revealed by DAPI staining. Images were acquired with the A1 HD25/ A1R HD25 laser scanning confocal microscope.

Immunohistochemical Staining

Frozen explant sections were rehydrated and blocked in 10% donkey serum for 1 hour, followed by incubation with rabbit polyclonal antibodies against Ki67 (1:300), Krt1 (1:300), PPAR-γ (1:100), IL-1β (1:200), ASC (1:200), and phospho-NF-κB p65 (1:200) overnight at 4°C. The next day, after a PBS wash for 15 minutes, frozen explant sections were incubated with Alexa Fluor 594, Donkey Anti-Rabbit IgG H&L (1:500) or Alexa Fluor 488, Donkey Anti-Rabbit IgG H&L (1:500) at 37°C for 60 minutes and then counterstained with DAPI. Images were obtained with the A1 HD25/ A1R HD25 laser scanning confocal microscope.

ELISA

The MG explants were cultured in 24-well plates and incubated with SACEs at 0.5, 1, or 2 µg/mL or treated with PBS (as vehicle control) for 48 hours. Finally, the supernatants were collected, and the mouse ELISA kit was used to detect the levels of TNF-α (430907; BioLegend, San Diego, USA) and IL-6 (431307; BioLegend).

RNA Extraction and Quantitative Reverse Transcription PCR

Total RNA of MG explants was extracted using TRIzol reagent (9108; TAKARA, Otsu, Shiga, Japan) according to the manufacturer's protocol, and an equal amount of RNA was reverse transcribed to cDNA using the PrimeScript RT Reagent Kit (RR047A; TAKARA). Subsequently, quantitative reverse transcription PCR (qRT-PCR) was performed on the StepOnePlus Real-Time PCR System (Life Technologies, Carlsbad; USA) and with a SYBR Premix Ex Taq kit (RR420A; TAKARA) according to the manufacturer's instructions. β-actin was used as the internal control, and the $2^{-\Delta\Delta Ct}$ method was used to evaluate the relative expression of mRNA. The sequences of primers used in this study were as follows:

Ki67, forward 5′-CTCACCTGGTCACCATCAAG -3′
Ki67, reverse 5′-TGTCACATTCAATACTCCTTCCA -3′
β-actin, forward 5′- TGCTGTCCCTGTATGCCTCTG -3′
β-actin, reverse 5′- TGATGTCACGCACGATTTCC-3′

Western Blot Analysis

MG explants were lysed in RIPA Lysis and Extraction Buffer (78440; Thermo Fisher Scientific) with 1% PMSF Protease Inhibitor (36978; Thermo Fisher Scientific). Protein concentration was measured using a BCA assay kit (23225; Thermo Fisher Scientific). Eight explants were used in each group. Equal amounts of protein extracts (25 µg), SEB protein (20 µg), and SACEs (30 µg) were separated by electrophoresis in sodium dodecyl sulfate–polyacrylamide gel electrophoresis (SDS-PAGE) gels and transferred to Immobilon-E polyvinylidene difluoride membrane (IEVH00005; MilliporeSigma, Burlington, MA, USA). Membranes were blocked with 5% milk or 5% BSA for 1 hour at room temperature. Membranes were then incubated with primary antibodies to β-actin (1:5000), GAPDH (1:5000), Ki67 (1:1000), Krt1 (1:1000), PPAR-γ (1:1000), LAMP-1 (1:1000), IL-1β (1:1000 31202S), pro-IL-1β (1:1000), caspase-1 (1:1000), pro-caspase-1 (1:1000), ASC (1:1000), anti-SEB antibody (1:1000), AIM2 (1:1000), and phospho-NF-κB p65 (1:1000) overnight at 4°C. After three washes with Tris-buffered saline containing 0.05% Tween 20 for 10 minutes, the membranes were incubated with HRP-conjugated goat anti-mouse or anti-rabbit IgG secondary antibodies for 1 hour at room temperature. Finally, the protein bands were detected by chemiluminescence using an electrochemiluminescence reagent (A38555; Thermo Fisher Scientific). SACEs (30 µg) were separated by electrophoresis in SDS-PAGE gel with the Pierce Silver Stain Kit (24612; Thermo Fisher Scientific). Staining intensities were quantified with ImageJ software (National Institutes of Health, Bethesda, MD, USA).

Statistical Analysis

SPSS Statistics 22.0.0 software (IBM, Armonk, NY, USA) was used for one-way ANOVA, post hoc Dunnett's *t*-test or Bonferroni's test was used for multiple groups, and *t*-tests were used for two groups. In this study, $P < 0.05$ was considered statistically significant. Data from at least three independent experiments are expressed as the mean ± SD.

Results

Influence of SACEs on the Mouse MG Explants

Previously, we established a MG organotypic culture in which the viability, morphology, and MG function were retained up to 72 hours.[16] Therefore, we chose to culture the explants in vitro for 48 hours in the current study. To determine the effect of SACEs on MG explants viability, we performed dose–response studies.

Tissue viability was detected by MTT assay, which showed that the relative OD values for the 1-µg/mL and 2-µg/mL SACEs treatments were 0.68 ± 0.03 and 0.59 ± 0.01, respectively, which were significantly lower than that for the control group ($P < 0.05$; $n = 6$ in each group) (Fig. 1A). Thus, the viability of mouse MG explants showed a dose-dependent decrease. H&E staining indicated that the ductal and acinar cells displayed vacuole degeneration at the concentration of 2 µg/mL SACEs (Fig. 1B). Taken together, the results suggest that SACEs suppressed the tissue viability of mouse MG explants in a dose-dependent manner.

Impact of SACEs Treatment on Keratinization and Pathological Change of Mouse MG Explants

Previous studies have shown a close correlation between MG loss and *S. aureus* abundance in patients with MGD.[12] We examined the effects of SACEs on mouse MG explants cell death and proliferation. The *Ki67* gene, a biomarker of high clonality and proliferation ability epithelial cells,[18] was apparently decreased in the SACEs-treated group compared with the control group, which was confirmed by western blot (Fig. 2A) and qRT-PCR analyses (Fig. 2C). Ki67 expression in the 2-µg/mL SACEs group showed a decrease of 66.45% in

Investigative Ophthalmology & Visual Science

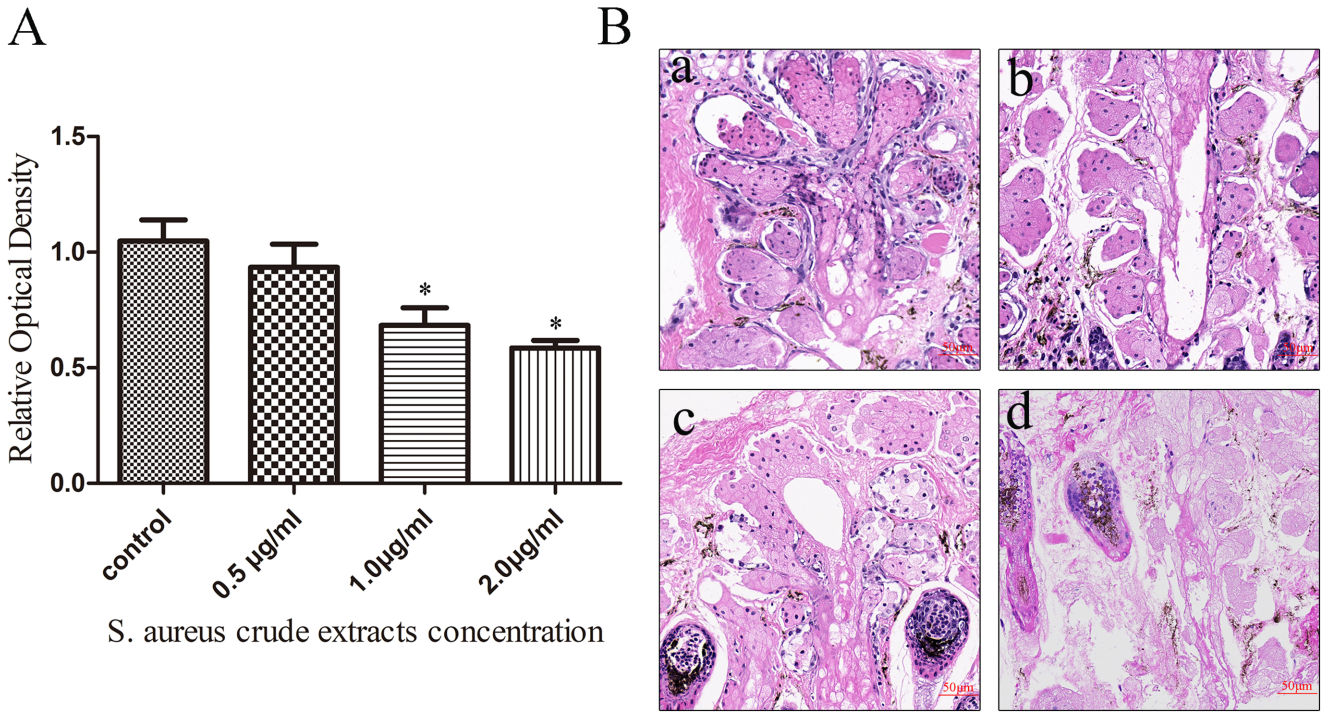

Figure 1. Viability of mouse MG explants for different concentrations of SACEs treatment. (**A**) MTT assay comparison of tissue viability in MG explants with different concentrations of SACEs ($n = 6$ in each group). The relative OD values of MG explants (each performed in triplicate) for SACEs treatments of 0, 0.5, 1, or 2 μg/mL as assessed by MTT assay are shown. (**B**) Morphology of MG explants at 0 μg/mL (**a**), 0.5 μg/mL (**b**), 1 μg/mL (**c**), and 2 μg/mL (**d**) by H&E staining. *Scale bars:* 50 μm. *Significantly different from the control group ($P < 0.05$).

protein level and 74.78% in mRNA level compared with the control group ($P < 0.05$; $n = 3$ in each group) (Figs. 2B, 2C).

Hyperkeratinization of the ductal orifice is the main pathological change for obstructive MGD.[19] As a biomarker for epithelial keratinization,[20] the expression of Krt1 was examined. Mouse MG explants were treated with 0.5, 1, or 2 μg/mL SACEs or vehicle for 48 hours. As illustrated in Figure 2D, Krt1 staining intensity was reinforced in the acinus and ducts when treated with high concentrations of SACEs (2 μg/mL). Compared with vehicle, 2-μg/mL SACEs treatment led to a 4.83-fold increase in the expression of Krt1 for the whole explants ($P < 0.05$; $n = 3$ in each group) (Figs. 2E, 2F).

Quantification of TUNEL-positive explants cells demonstrated increased cell death in the 1-μg/mL and the 2-μg/mL SACE-treated explants compared with the control group ($P < 0.05$, $n = 3$ in each group) (Figs. 2G, 2H). These results indicated that SACEs induced cell death in mouse MGs explants in a dose-dependent manner.

Impact of SACEs Treatment on Lipid Droplet Formation in Mouse MG Explants

To determine whether SACEs are associated with lipid synthesis in MG, we treated mouse MG explants with 0.5, 1, or 2 μg/mL SACEs or vehicle for 48 hours and conducted LipidTOX assays and Nile Red staining. LipidTOX results showed that there was no change in lipid accumulation in mouse MG under treatment ($P > 0.05$; $n = 3$ in each group) (Figs. 3A, 3B). The relative Nile Red staining results were consistent with the LipidTOX results ($P > 0.05$; $n = 3$ in each group) (Figs. 3C, 3D).

Influence of SACEs on the Expression of Protein Biomarkers of Differentiation in MG Explants

The terminal differentiation of meibocytes in the MG is preserved by PPAR-γ, which acts as a regulator of lipid synthesis.[21,22] Immunofluorescence staining indicated that nuclear and cytoplasmic staining of PPAR-γ in SACEs-treated explants was decreased (Fig. 4A). Consistent with our immunofluorescence results, PPAR-γ expression in the 2-μg/mL SACEs group was decreased by 47.04% compared with the control group ($P < 0.05$; $n = 3$ in each group) (Figs. 4B, 4C). LAMP-1 is a biomarker for lysosomes.[23] To test whether SACEs could influence differentiation of mouse MG explants, we treated explants with 0.5, 1, or 2 μg/mL SACEs or vehicle as a control for 48 hours and analyzed the explants for LAMP-1 expression. As shown in Figures 4D and 4E, with increasing concentrations of SACEs the expression of LAMP-1 showed no significant change ($P > 0.05$; $n = 3$ in each group).

Cytokine Expression and Caspase-1 Activation Were Dose Dependent in MG Explants

Previous studies have shown that the MG cells secrete TNF-α, IL-1β, and IL-6 under 13-*cis* retinoic acid or hyperlipidemia stimulation.[24,25] We determined the levels of TNF-α, IL-1β, and IL-6 in mouse MG explants to determine whether SACEs affect the production of these proinflammatory

Investigative Ophthalmology & Visual Science

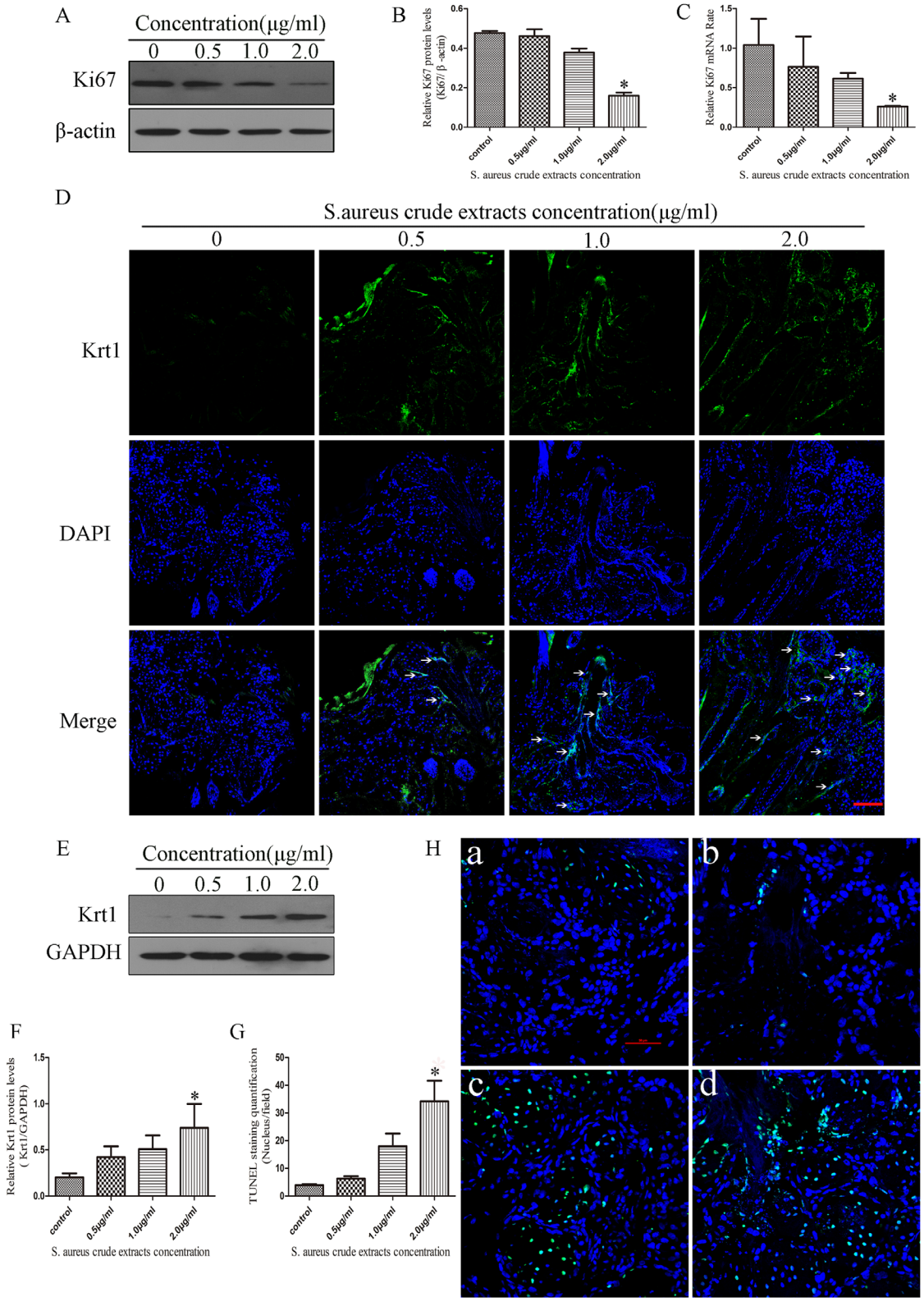

Figure 2. Reduced proliferation, hyperkeratinization, and increased cell death in mouse MG explants with SACEs treatment. Western blot (**A**, **B**) and qRT-PCR analysis (**C**) indicated that the gene expression of Ki67 was apparently decreased in the SACEs treatment group compared with the control group. Images show that Krt1-positive cells increased in acinar and ductal cells of mouse MG explants with increasing concentrations of SACEs (**D**, *arrow head*). *Scale bars:* 100 µm. Western blot analysis indicated that Krt1 was also upregulated (**E**, **F**). Increased TUNEL assay staining (**H**) and cell counts (**G**) suggest increased cell deaths in the SACEs treatment groups—0.5 µg/mL (**Hb**); 1 µg/mL (**Hc**); and 2 µg/mL (**Hd**)—compared with those of the control group: 0 µg/mL (**Ha**). *Scale bars:* 50 µm. Bar graphs show the statistical analysis of three independent experiments (*$P < 0.05$). Krt1, *green*; DAPI, *blue*; TUNEL, *green*.

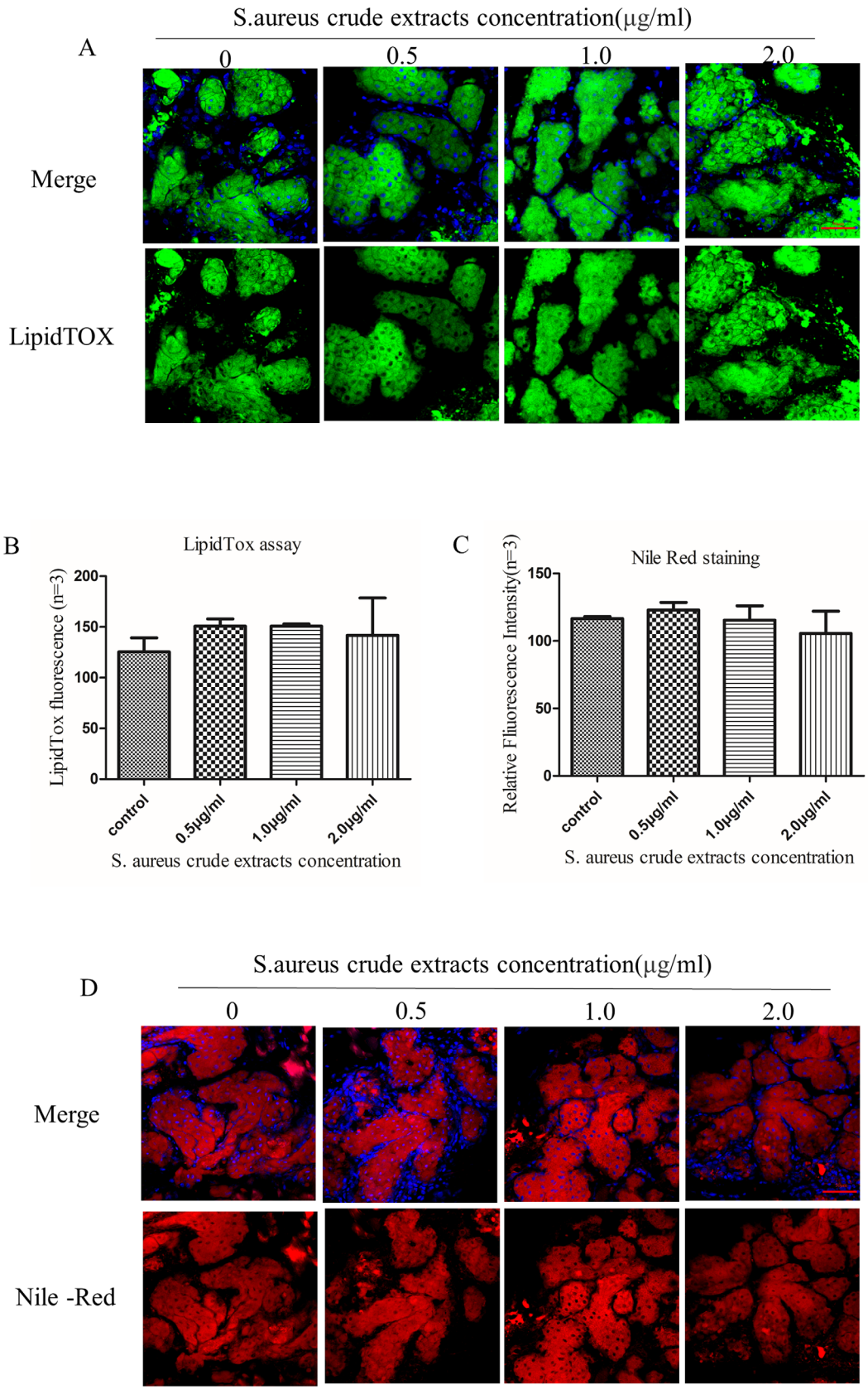

Figure 3. Influence of SACEs treatment on neutral lipid accumulation in mouse MG explants. Nile Red staining and LipidTox assays were performed after 48 hours of SACEs treatment. Lipid droplets were stained with LipidTox (**A**) and Nile Red staining (**D**), and the results of the LipidTox assay and Nile Red staining are summarized (**B**, **C**). Data are represented as the mean ± SD (*$P < 0.05$). *Scale bars:* 50 μm. LipidTox, *green*; Nile Red, *red*; DAPI, *blue*.

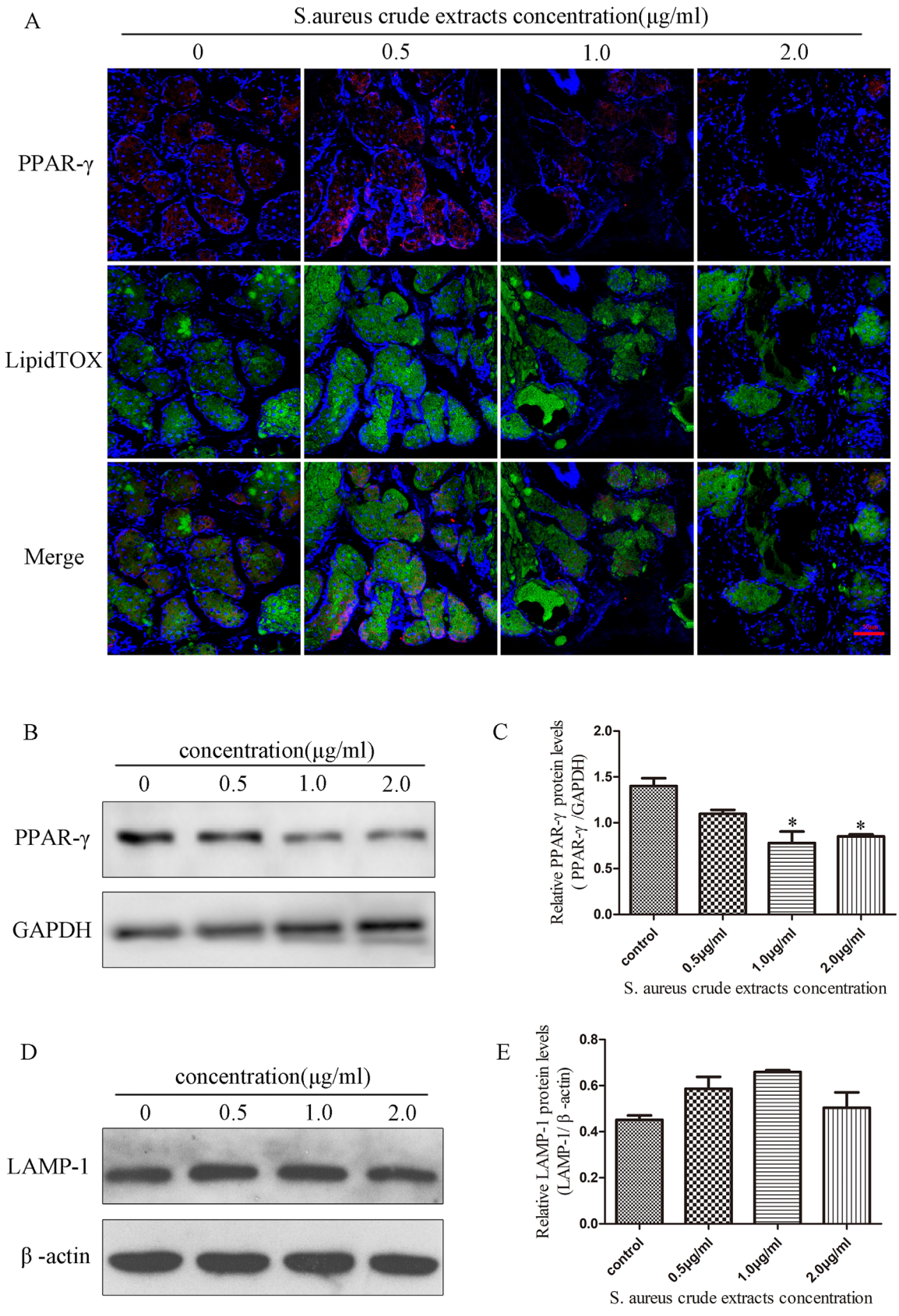

Figure 4. Influence of SACEs treatment on the expression of PPAR-γ and LAMP-1 in mouse MG explants. Immunofluorescence of PPAR-γ (**A**) and western blot analysis (**B**, **C**) showed a decrease in the SACEs treatment group compared with the control group. Western blot analysis (**D**, **E**) indicated that the expression of LAMP-1 showed no significant change with increasing concentrations of SACEs. Data are represented as the mean ± SD of three independent experiments (*$P < 0.05$). *Scale bars:* 50 µm. PPAR-γ, *red*; DAPI, *blue*; LipidTox, *green*.

Investigative Ophthalmology & Visual Science

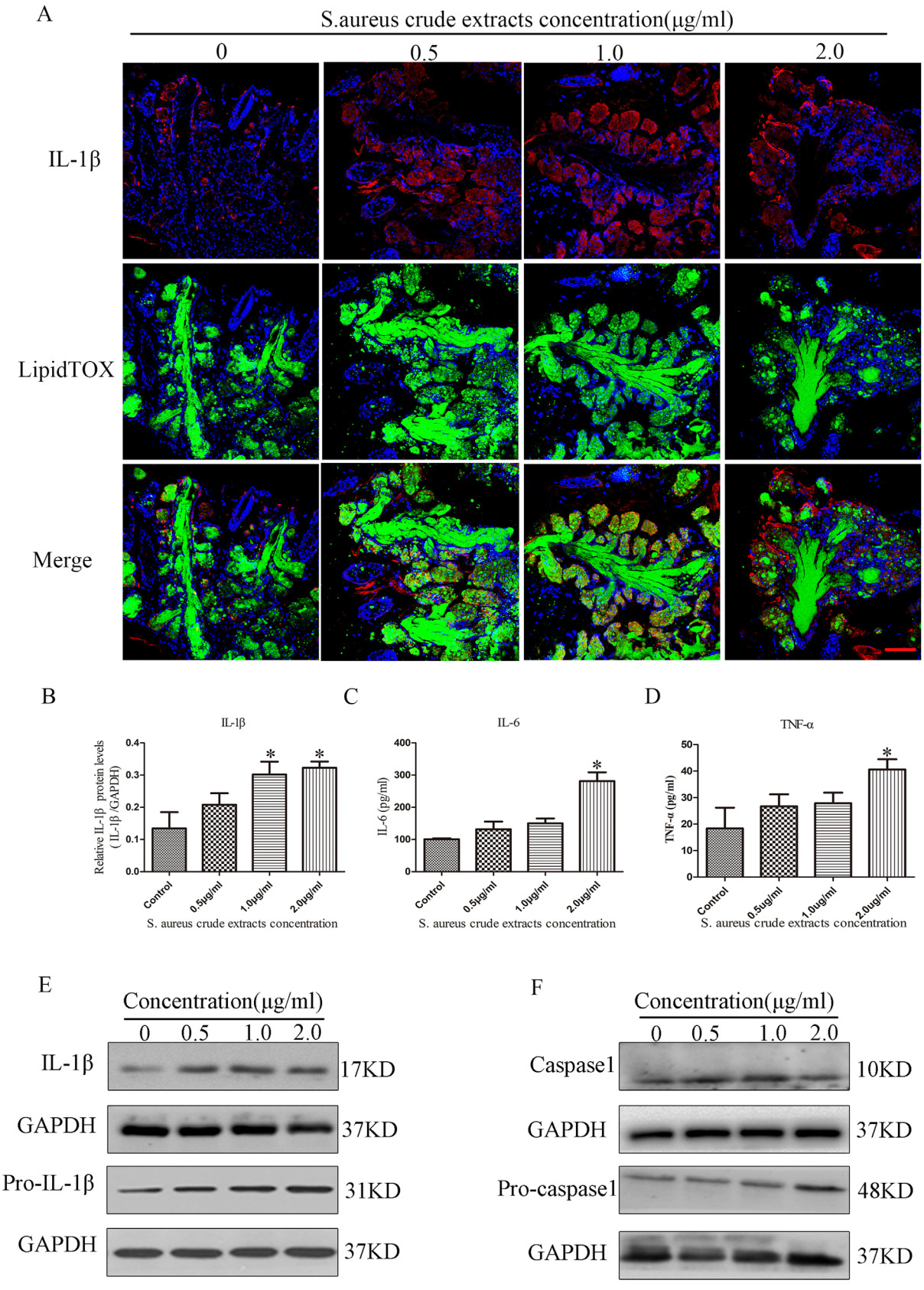

Figure 5. SACEs induced caspase-1 activation and cytokine secretion in mouse MG explants. (**A**) Immunofluorescence staining analysis of IL-1β in explants for SACEs treatments of 0, 0.5, 1, or 2 μg/mL. (**B**, **E**, **F**) Immunoblotting analysis of pro-caspase-1, caspase-1, pro-IL-1β, and IL-1β in explants for SACEs treatments of 0, 0.5, 1, or 2 μg/mL. (**C**, **D**) The production of IL-6 and TNF-α was measured by ELISA. *Significantly different from the control group ($P < 0.05$). *Scale bars:* 100 μm. IL-1β, *red*; DAPI, *blue*; LipidTox, *green*.

Investigative Ophthalmology & Visual Science

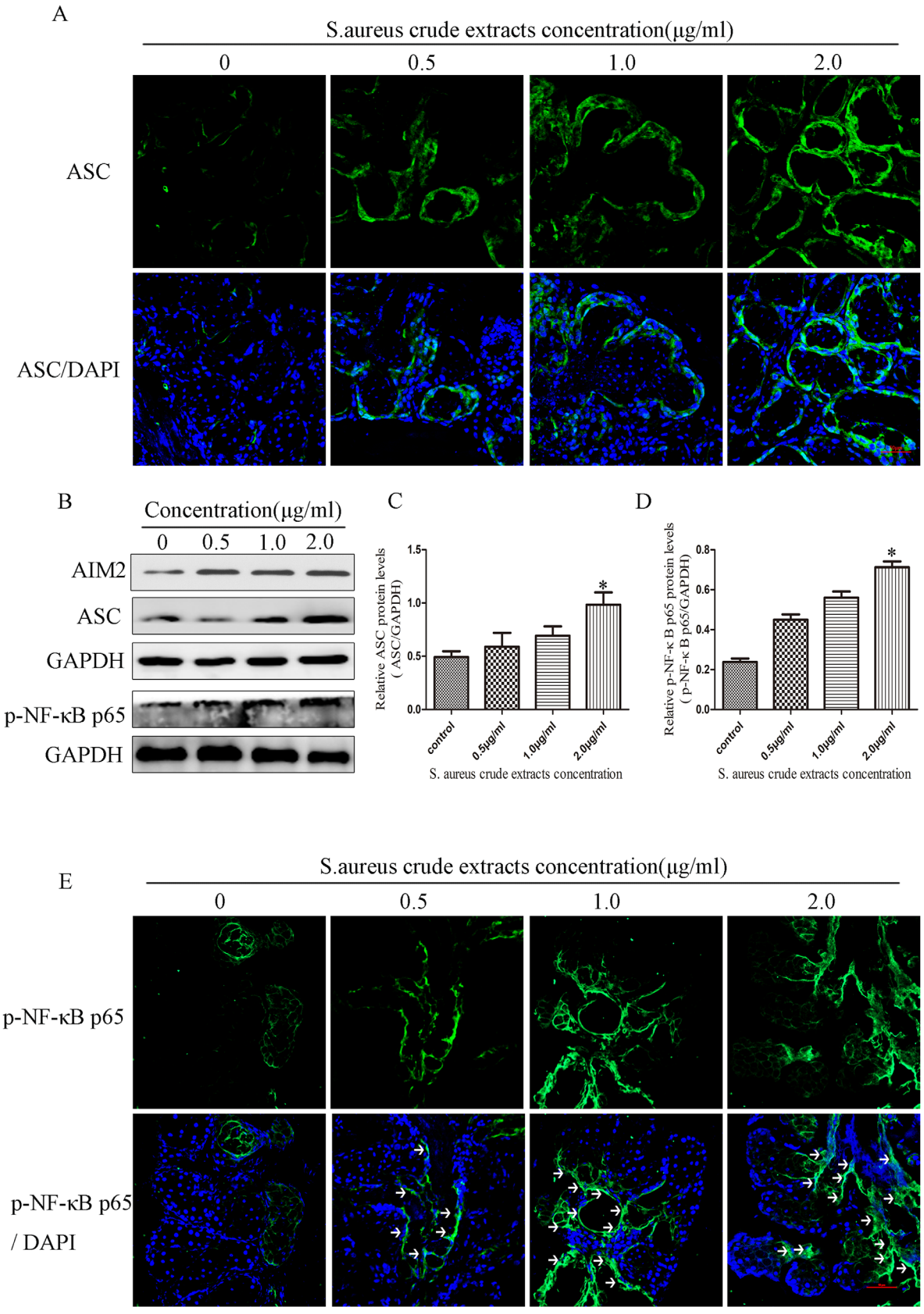

Figure 6. SACEs upregulated the protein expression of ASC and phospho-NF-κB p65. Immunofluorescence staining analysis of ASC (**A**) and phospho-NF-κB p65 (**E**, *arrowhead*) in explants for SACEs treatments of 0, 0.5, 1, or 2 μg/mL. Protein levels of AIM2, ASC, and phospho-NF-κB p65 indicated significant upregulation in mouse MG explants with SACEs treatment compared with the control group (**B–D**). *Scale bars:* 50 μm. *Significantly different from the control group ($P < 0.05$). ASC and phospho-NF-κB p65, *green*; DAPI, *blue*.

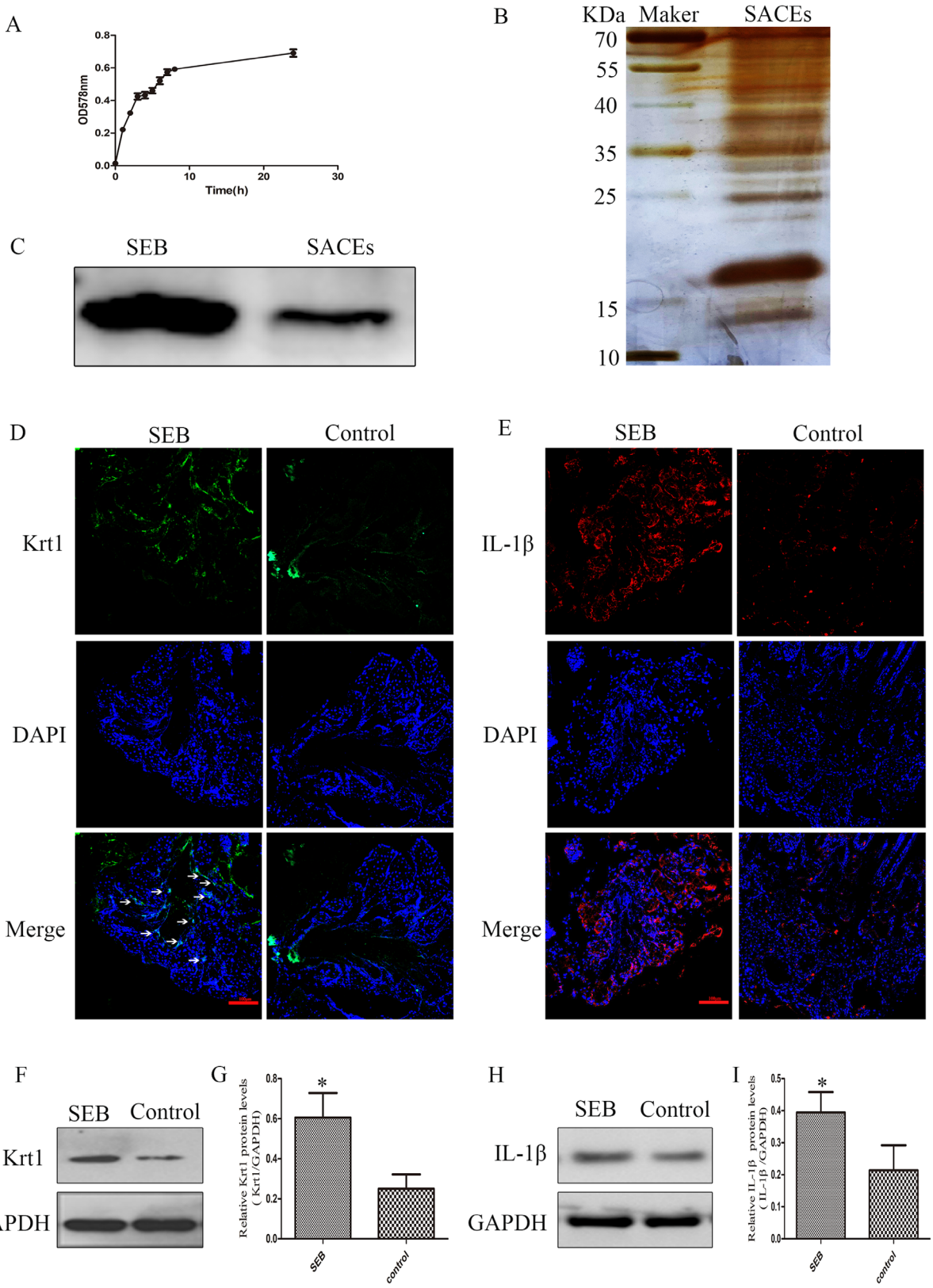

Figure 7. Keratinization and IL-1β expression of SACEs by mouse MG explants depended on SEB. (**A**) Growth curve of *S. aureus* ATCC 29213. (**B**) The components of the SACEs were analyzed by immunoblotting and silver staining. (**C**) Western blotting results showed that the SACEs contained SEB. Immunofluorescence of Krt1 (**D**) and western blot analysis (**F**, **G**) indicated increases in the SEB treatment group compared with the control group. Immunofluorescence of IL-1β (**E**) and western blot analysis (**H**, **I**) showed increases in the SEB treatment group compared with the control group. *Scale bars:* 100 µm. *Significantly different from the control group ($P < 0.05$). Krt1, *green*; IL-1β, *red*; DAPI, *blue*.

cytokines. Immunofluorescence staining of frozen MG explants showed that IL-1β production increased following treatment with SACEs (Fig. 5A). Consistent with our immunofluorescence results, IL-1β expression in the 2-µg/mL SACEs group was increased by 1.93-fold compared with the control group ($P < 0.05$; $n = 3$ in each group) (Figs. 5B, 5E). ELISA results showed that the levels of IL-6 and TNF-α for high concentrations of SACEs (2 µg/mL) were significantly higher than in the control group (Figs. 5C, 5D).

Caspase-1 is a cysteine protease that induces the conversion of immature IL-1β (*P*ro-IL-1β) into mature IL-1β.[26] To investigate the role of caspase-1 cleavage on IL-1β secretion in SACEs-treated explants, we treated mouse MG explants with 0.5, 1, and 2 µg/mL SACEs or vehicle for 48h and then examined the cleavage of caspase-1 by western blot. We found that SACEs led to the cleavages of pro-IL-1β to IL-1β and of pro-caspase-1 to caspase-1, with increasing concentrations of SACEs (Figs. 5E, 5F). These results suggested that SACEs induced IL-1β expression and it depends on caspase-1 activation in mouse MG explants.

Impact of SACEs on the AIM2/ASC Signaling Pathway and NF-κB Pathway

The inflammasome is a multiprotein complex composed of sensor-receptor protein, apoptosis-related ASC, and cysteine protease caspase-1.[27] After activation, it can promote the release of mature IL-1β, which plays a crucial role in the innate immune response against invading microorganisms.[27–29] The fluorescence intensities of ASC (Fig. 6A) and phospho-NF-κB p65 (Fig. 6E) in the 2-µg/mL SACEs group were enhanced sharply compared with the control group. Immunoblotting also revealed that the SACEs induced upregulation of AIM2, ASC, and phospho-NF-κB p65 on mouse MG explants (Fig. 6B). ASC and phospho-NF-κB p65 expression in the 2-µg/mL SACEs group was increased by 2.02-fold and 2.17-fold, respectively, compared with the control group ($P < 0.05$; $n = 3$ in each group) (Figs. 6C, 6D). These results indicate that SACEs induced caspase-1 activation, to some extent, through an enhancement of the AIM2/ASC pathway in the mouse MG. Secretion of the pro-inflammatory factors might also be correlated with the NF-κB pathway.

Keratinization and IL-1β Expression of SACEs by Mouse MG Explants Depends on SEB

Exotoxins are produced by *S. aureus* in a growth-phase–dependent manner, primarily during the post-exponential phase of growth[30] in which bacteria were collected. The growth curve of *S. aureus* ATCC 29213 is shown in Figure 7A. To investigate the role of SACEs, we performed western blotting and silver staining on SACEs. Silver staining revealed multiple bands ranging from 15 to 35 kDa (Fig. 7B). Western blotting showed that the SACEs contained SEB (Fig. 7C). We further studied the effect of SEB on MG keratinization and the production of proinflammatory cytokines. We treated mouse MG explants with 0.5 µg/mL SEB or vehicle for 48 hours. The fluorescence intensities of Krt1 (Fig. 7D) and IL-1β (Fig. 7E) in the 0.5-µg/mL SEB group were enhanced sharply compared with the control group. Compared with vehicle, SEB led to 3.56-fold and 1.93-fold increases in the expression of Krt1 and IL-1β, respectively, of the whole explants ($P < 0.05$, $n = 3$ in each group) (Figs. 7F–7I). Thus, SEB released by *S. aureus* may play an essential role in secretion of IL-1β and keratinization in MG explants.

Discussion

Our results demonstrate that mouse MG explants exposure to SACEs causes a dose-dependent increase in cell death and hyperkeratinization of the acini and ducts. SACEs reduced the expression of PPAR-γ proteins. In contrast, SACEs had no influence on lipid synthesis in MG explants. SACEs also induced inflammation and significantly increased the expression of pro-inflammatory cytokines, including TNF-α, IL-1β, and IL-6, as well as the activated AIM2/ASC pathway and NF-κB pathway. Furthermore, inflammation and hyperkeratinization might be somewhat mediated by SEB. Overall, these results support our hypothesis that *S. aureus* affects MG explant morphology, survival, and proliferative capacity.

S. aureus secreted various toxins, many of which reportedly trigger cell death. Another important observation was the positive correlation between *S. aureus* abundance and MG loss in patients with MGD.[12] In the present study, SACEs treatment resulted in vacuole degeneration in explants cells, consistent with results reported in MGD patients.[31] Ki67 expression supported the decreased proliferation of explants cells. TUNEL staining indicated an elevated number of acinar and ductal cell deaths.

The main pathological changes of obstructive MGD were keratinization of ducts and acinus, which can lead to degraded gland expansion and atrophy.[3,32–34] In our study, SACEs upregulated Krt1 expression in ductal and acinar cells. As a terminally keratinized epithelium marker, Krt1 is only found in the excretory duct, which lined by an ingrowth of the cornified epidermis from the lid margin.[3,20] These results indicate that SACEs might induce ductal and acinar hyperkeratinization, leading to obstructive MGD.

It is generally accepted that lipase secreted by bacteria may be one of the factors affecting the composition of meibum.[14] Meibum alteration often results in increased lipid viscosity and decreased fluidity and obstruction of the ductal orifice and becomes useful for the excessive growth of inherent microorganisms in catheters.[10,35] Several studies have reported a substantial increase in overall neutral lipid accumulation of immortalized human meibomian gland epithelial cells (IHMGECs) when treated with azithromycin[36,37] and recombinant insulin-like growth factor-I[38] for approximately 7 days.[39] Lipid accumulation in IHMGECs appeared to occur in lysosomes.[40] LAMP-1 is a biomarker for lysosomes[23]; however, in our study, SACEs had no influence on the levels of LAMP-1 or lipid droplets. Possible reasons may include different culture times. This is a limitation of our research that requires further investigation.

We found that the decrease of PPAR-γ played an important role in lipid synthesis of the sebaceous gland.[41–43] Indeed, PPAR-γ–dependent signaling plays an essential role in the control of inflammation.[44] In part, the downregulation of PPAR-γ may be connected with the inflammatory nature of the explants. Furthermore, lipoproteins of *S. aureus* are known to induce IL-1β and IL-6 production in epithelial cells.[45,46] In our study, SACEs significantly increased the expression of various inflammatory mediators, including IL-1β, IL-6, and TNF-α, in mouse MG explants, all of which have been related to the pathophysiology of dry eye disease.[47–49] IL-1β is the primary proinflammatory cytokine that regulates inflammation at local and systemic levels.[50,51] Our previous

Investigative Ophthalmology & Visual Science

research reported that IL-1β induced a significant hyperkeratinization of ducts.[16] In addition, as an inflammatory mediator of the ocular surface, IL-1β was also involved in cell death regulation.[52] Thus, SACEs may promote MG epithelial cell death and hyperkeratinization, at least in part, via IL-1β. NF-κB has a vital function in regulating innate immunity and inflammation.[53,54] When the NF-κB pathway is activated, the p65 unit separates from IκB-α,[55] which inhibits the signaling factor; NF-κB then transfers from the cytoplasm to the nucleus, where it may trigger TNF-α, IL-1β, and IL-6. Taken together, results of our study indicate that the NF-κB signaling pathway was activated in the explants.

We investigated the effect of SACEs in inflammasome stimulation in mouse MGs. *S. aureus* virulence factors have been reported to induce multiple inflammasomes.[56] The cleavage of pro-caspase-1 to caspase-1 and of pro-IL-1β to IL-1β is considered a hallmark of inflammasome activation.[57] Our results indicated that a higher concentration (2 µg/mL) of SACEs increased the expression of the adapter protein AIM2 and ASC, accompanied by expression of caspase-1 and IL-1β. This pro-inflammatory effect of ASC inflammasome activation may directly affect the maturation of IL-1β in mouse MG explants with SACEs treatment.

Previous studies have reported that *S. aureus* ocular clinical strains were found to be significantly enriched for a set of enterotoxins, and genomic analysis revealed that these enterotoxins were located on mobile pathogenicity islands; thus, horizontal gene transfer may promote the acquisition of enterotoxins, potentially amplifying *S. aureus* virulence in ocular tissues.[58] Although there are more than 20 distinct staphylococcal enterotoxins, the most common staphylococcal enterotoxins are staphylococcal enterotoxins A and SEB. Ocular surface exposure to SEB can occur during extraocular staphylococcal infections such as keratitis, conjunctivitis, blepharitis, or atopic keratoconjunctivitis, albeit in smaller amounts.[58] SEB have been shown to be toxic to corneal epithelial cells and to induce changes in cytokine expression in an in vitro cell culture model.[59] In our study, SEB induced keratinization and the expression of IL-1β. However, silver staining on the SACEs showed that most of the proteins had molecular weights between 15 $\sim$ 35 kDa. The major exotoxins secreted by *S. aureus* include α-toxin (33 kDa), enterotoxins, and toxic shock syndrome toxin 1 (20$\sim$30 kDa). These toxins may work at the same time. The composition of SACEs and their influence on explants require further investigation.

In conclusion, our findings demonstrate that *S. aureus* induced MG hyperkeratinization, abnormal MG ductal and acinar cell differentiation, cell death, and increased expression of inflammatory factor. These findings facilitate an understanding of the role of *S. aureus* in MGD.

Acknowledgments

Supported by the National Key Research and Development Program of China (2017YFE0103500) and the National Natural Science Foundation of China (81670824 and 82070934).

Disclosure: **H. Chen**, None; **H. Gao**, None; **H.-T. Xie**, None; **S.-T. Liu**, None; **Y.-K. Huang**, None; **M.-C. Zhang**, None

References

1. Jester JV, Nicolaides N, Smith RE. Meibomian gland studies: histologic and ultrastructural investigations. *Invest Ophthalmol Vis Sci*. 1981;20(4):537–547.
2. Suzuki T, Sutani T, Nakai H, Shirahige K, Kinoshita S. The microbiome of the meibum and ocular surface in healthy subjects. *Invest Ophthalmol Vis Sci*. 2020;61(2):18.
3. Knop E, Knop N, Millar T, Obata H, Sullivan DA. The international workshop on meibomian gland dysfunction: report of the subcommittee on anatomy, physiology, and pathophysiology of the meibomian gland. *Invest Ophthalmol Vis Sci*. 2011;52(4):1938–1978.
4. Nelson JD, Shimazaki J, Benitez-del-Castillo JM, et al. The international workshop on meibomian gland dysfunction: report of the definition and classification subcommittee. *Invest Ophthalmol Vis Sci*. 2011;52(4):1930–1937.
5. Green-Church KB, Butovich I, Willcox M, et al. The international workshop on meibomian gland dysfunction: report of the subcommittee on tear film lipids and lipid-protein interactions in health and disease. *Invest Ophthalmol Vis Sci*. 2011;52(4):1979–1993.
6. Zhang SD, He JN, Niu TT, et al. Bacteriological profile of ocular surface flora in meibomian gland dysfunction. *Ocul Surf*. 2017;15(2):242–247.
7. Bernardes TF, Bonfioli AA. Blepharitis. *Semin Ophthalmol*. 2010;25(3):79–83.
8. Lee SH, Oh DH, Jung JY, Kim JC, CO Jeon. Comparative ocular microbial communities in humans with and without blepharitis. *Invest Ophthalmol Vis Sci*. 2012;53(9):5585–5593.
9. Watters GA, Turnbull PR, Swift S, Petty A, Craig JP. Ocular surface microbiome in meibomian gland dysfunction. *Clin Exp Ophthalmol*. 2017;45(2):105–111.
10. Jiang X, Deng A, Yang J, et al. Pathogens in the meibomian gland and conjunctival sac: microbiome of normal subjects and patients with meibomian gland dysfunction. *Infect Drug Resist*. 2018;11:1729–1740.
11. Yarwood JM, Schlievert PM. Quorum sensing in *Staphylococcus* infections. *J Clin Invest*. 2003;112(11):1620–1625.
12. Dong X, Wang Y, Wang W, Lin P, Huang Y. Composition and diversity of bacterial community on the ocular surface of patients with meibomian gland dysfunction. *Invest Ophthalmol Vis Sci*. 2019;60(14):4774–4783.
13. Mudgil P. Antimicrobial role of human meibomian lipids at the ocular surface. *Invest Ophthalmol Vis Sci*. 2014;55(11):7272–7277.
14. Dougherty JM, McCulley JP. Bacterial lipases and chronic blepharitis. *Invest Ophthalmol Vis Sci*. 1986;27(4):486–491.
15. Stoll H, Dengjel J, Nerz C, Götz F. *Staphylococcus aureus* deficient in lipidation of prelipoproteins is attenuated in growth and immune activation. *Infect Immun*. 2005;73(4):2411–2423.
16. Xu KK, Huang YK, Liu X, Zhang MC, Xie HT. Organotypic culture of mouse meibomian gland: a novel model to study meibomian gland dysfunction in vitro. *Invest Ophthalmol Vis Sci*. 2020;61(4):30.
17. Kim KH, Han JH, Chung JH, Cho KH, Eun HC. Role of staphylococcal superantigen in atopic dermatitis: influence on keratinocytes. *J Korean Med Sci*. 2006;21(2):315–323.
18. Gerdes J, Schwab U, Lemke H, Stein H. Production of a mouse monoclonal antibody reactive with a human nuclear antigen associated with cell proliferation. *Int J Cancer*. 1983;31(1):13–20.
19. Gutgesell VJ, Stern GA, Hood CI. Histopathology of meibomian gland dysfunction. *Am J Ophthalmol*. 1982;94(3):383–387.
20. Parfitt GJ, Xie Y, Reid KM, et al. A novel immunofluorescent computed tomography (ICT) method to localise and quantify multiple antigens in large tissue volumes at high resolution. *PLoS One*. 2012;7(12):e53245.
21. Parfitt GJ, Xie Y, Reid KM, Dervillez X, Brown DJ, Jester JV. A novel immunofluorescent computed tomography

(ICT) method to localise and quantify multiple antigens in large tissue volumes at high resolution. *PLoS One.* 2012;7(12):e53245.

22. Jester JV, Potma E, Brown DJ. PPARγ regulates mouse meibocyte differentiation and lipid synthesis. *Ocul Surf.* 2016;14(4):484–494.
23. Eskelinen EL. Roles of LAMP-1 and LAMP-2 in lysosome biogenesis and autophagy. *Mol Aspects Med.* 2006;27(5-6):495–502.
24. Bu J, Wu Y, Cai X, et al. Hyperlipidemia induces meibomian gland dysfunction. *Ocul Surf.* 2019;17(4):777–786.
25. Ding J, Kam WR, Dieckow J, Sullivan DA. The influence of 13-*cis* retinoic acid on human meibomian gland epithelial cells. *Invest Ophthalmol Vis Sci.* 2013;54(6):4341–4350.
26. Kahlenberg JM, Lundberg KC, Kertesy SB, Qu Y, Dubyak GR. Potentiation of caspase-1 activation by the P2X7 receptor is dependent on TLR signals and requires NF-kappaB-driven protein synthesis. *J Immunol.* 2005;175(11):7611–7622.
27. Kovacs SB, Miao EA. Gasdermins: effectors of pyroptosis. *Trends Cell Biol.* 2017;27(9):673–684.
28. Wu T, Liu W, Fan T, et al. 5-Androstenediol prevents radiation injury in mice by promoting NF-κB signaling and inhibiting AIM2 inflammasome activation. *Biomed Pharmacother.* 2020;121:109597.
29. Schroder K, Tschopp J. The inflammasomes. *Cell.* 2010;140(6):821–832.
30. Arvidson S, Tegmark K. Regulation of virulence determinants in *Staphylococcus aureus*. *Int J Med Microbiol.* 2001;291(2):159–170.
31. Arita R, Itoh K, Inoue K, Amano S. Noncontact infrared meibography to document age-related changes of the meibomian glands in a normal population. *Ophthalmology.* 2008;115(5):911–915.
32. Gutgesell VJ, Stern GA, Hood CI. Histopathology of meibomian gland dysfunction. *Am J Ophthalmol.* 1982;94(3):383–387.
33. Jester JV, Rife L, Nii D, et al. In vivo biomicroscopy and photography of meibomian glands in a rabbit model of meibomian gland dysfunction. *Invest Ophthalmol Vis Sci.* 1982;22(5):660–667.
34. Jester JV, Rajagopalan S, Rodrigues M. Meibomian gland changes in the rhino (br^{rb}/br^{rb}) mouse. *Invest Ophthalmol Vis Sci.* 1988;29(7):1190–1194.
35. Baudouin C, Messmer EM, Aragona P, et al. Revisiting the vicious circle of dry eye disease: a focus on the pathophysiology of meibomian gland dysfunction. *Br J Ophthalmol.* 2016;100(3):300–306.
36. Liu Y, Kam WR, Ding J, Sullivan DA. Effect of azithromycin on lipid accumulation in immortalized human meibomian gland epithelial cells. *JAMA Ophthalmol.* 2014;132(2):226–228.
37. Liu Y, Kam WR, Ding J, Sullivan DA. One man's poison is another man's meat: using azithromycin-induced phospholipidosis to promote ocular surface health. *Toxicology.* 2014;320:1–5.
38. Ding J, Sullivan DA. The effects of insulin-like growth factor 1 and growth hormone on human meibomian gland epithelial cells. *JAMA Ophthalmol.* 2014;132(5):593–599.
39. Liu S, Hatton MP, Khandelwal P, Sullivan DA. Culture, immortalization, and characterization of human meibomian gland epithelial cells. *Invest Ophthalmol Vis Sci.* 2010;51(8):3993–4005.
40. Sullivan DA, Liu Y, Kam WR, et al. Serum-induced differentiation of human meibomian gland epithelial cells. *Invest Ophthalmol Vis Sci.* 2014;55(6):3866–3877.
41. Imai T, Takakuwa R, Marchand S, et al. Peroxisome proliferator-activated receptor gamma is required in mature white and brown adipocytes for their survival in the mouse. *Proc Natl Acad Sci USA.* 2004;101(13):4543–4547.
42. Nien CJ, Massei S, Lin G, et al. The development of meibomian glands in mice. *Mol Vis.* 2010;16:1132–1140.
43. Gervois P, Fruchart JC, Staels B. Inflammation, dyslipidaemia, diabetes and PPars: pharmacological interest of dual PPARalpha and PPARgamma agonists. *Int J Clin Pract Suppl.* 2004(143):22–29.
44. Delerive P, Fruchart JC, Staels B. Peroxisome proliferator-activated receptors in inflammation control. *J Endocrinol.* 2001;169(3):453–459.
45. Xue M, Jackson CJ. Autocrine actions of matrix metalloproteinase (MMP)-2 counter the effects of MMP-9 to promote survival and prevent terminal differentiation of cultured human keratinocytes. *J Invest Dermatol.* 2008;128(11):2676–2685.
46. Hoene M, Weigert C. The role of interleukin-6 in insulin resistance, body fat distribution and energy balance. *Obes Res.* 2008;9(1):20–29.
47. The epidemiology of dry eye disease: report of the Epidemiology Subcommittee of the International Dry Eye WorkShop (2007). *Obes Res.* 2008;9(1):20–29.
48. Solomon A, Dursun D, Liu Z, et al. Pro- and anti-inflammatory forms of interleukin-1 in the tear fluid and conjunctiva of patients with dry-eye disease. *Invest Ophthalmol Vis Sci.* 2001;42(10):2283–2292.
49. Luo L, Li DQ, Doshi A, et al. Experimental dry eye stimulates production of inflammatory cytokines and MMP-9 and activates MAPK signaling pathways on the ocular surface. *Invest Ophthalmol Vis Sci.* 2001;42(10):2283–2292.
50. Wright JG, Christman JW. The role of nuclear factor kappa B in the pathogenesis of pulmonary diseases: implications for therapy. *Am J Respir Med.* 2003;2(3):211–219.
51. McCoy MK, Ruhn KA, Blesch A, Tansey MG. TNF: a key neuroinflammatory mediator of neurotoxicity and neurodegeneration in models of Parkinson's disease. *Adv Exp Med Biol.* 2011;691:539–540.
52. Baeza-Raja B, Goodyear A, Liu X, et al. Pharmacological inhibition of P2RX7 ameliorates liver injury by reducing inflammation and fibrosis. *PLoS One.* 2020;15(6):e0234038.
53. Li Q, Verma IM. NF-kappaB regulation in the immune system. *Nat Rev Immunol.* 2002;2(10):725–734.
54. Baker RG, Hayden MS, Ghosh S. NF-κB, inflammation, and metabolic disease. *Cell Metab.* 2011, 13(1):11–22.
55. Brasier AR. The NF-kappaB regulatory network. *Cardiovasc Toxicol.* 2006;6(2):111–130.
56. Hanamsagar R, Aldrich A, Kielian T. Critical role for the AIM2 inflammasome during acute CNS bacterial infection. *J Neurochem.* 2014;129(4):704–711.
57. Franchi L, Eigenbrod T, Muñoz-Planillo R, Nuñez G. The inflammasome: a caspase-1-activation platform that regulates immune responses and disease pathogenesis. *Nat Immunol.* 2009;10(3):241–247.
58. Johnson WL, Sohn MB, Taffner S, et al. Genomics of *Staphylococcus aureus* ocular isolates. *PLoS One.* 2021;16(5):e0250975.
59. Thakur A, Clegg A, Chauhan A, Willcox MD. Modulation of cytokine production from an EpiOcular corneal cell culture model in response to *Staphylococcus aureus* superantigen. *Aust N Z J Ophthalmol.* 1997;25(suppl 1):S43–S45.

Investigative Ophthalmology & Visual Science